Convection, Diffusion and Reaction in a Nonisothermal, Porous Catalyst Slab

Silvana S. S. Cardoso
Dept. of Chemical Engineering, University of Cambridge, Cambridge CB2 3RA, U.K.

Alírio E. Rodrigues
LSRE, Departamento de Engenharia Química, Faculdade de Engenharia da Universidade do Porto, Rua Dr. Roberto Frias, 4200-465 Porto, Portugal

DOI 10.1002/aic.11158
Published online March 27, 2007 in Wiley InterScience (www.interscience.wiley.com).

The problem of simultaneous convection, diffusion and reaction inside a porous catalyst slab is considered. A combination of perturbation and integral mathematical techniques are used to derive approximate analytical solutions for the concentration and temperature profiles, as well as for the maximum temperature and the effectiveness factor, for a first order, nonisothermal reaction. Three regimes of operation are characterized: regime I, in which convection and diffusion are dominant (small Thiele modulus); regime II, in which diffusion and reaction are dominant (large Thiele modulus); and regime III, in which convection and reaction dominate (intermediate Thiele modulus). Our analytical solutions for each of these regimes are validated by comparison with previous results from numerical simulations. © 2007 American Institute of Chemical Engineers *AIChE J,* 53: 1325–1336, 2007

Keywords: catalysis, reaction kinetics, mathematical modeling, porous media, transport

Introduction

The coupling of chemical reaction and diffusive transport in porous catalytic particles has been the subject of intense investigation in chemical engineering for many years. In his treatise, *The Mathematical Theory of Diffusion and Reaction in Permeable Catalysts*, Rutherford Aris[1] presented a comprehensive review of the literature up to 1975. Since then, a number of scientific publications have considered the effect of transport by convection, in addition to diffusion, inside porous catalyst particles undergoing chemical reaction.

Indeed, several studies have shown that intraparticle convection in large-pore catalysts (with pore diameters above 500 Å) can contribute significantly to the total transport rate inside the particle. As early as 1951, Wheeler[2] conceived that forced convective flow might occur within the pores of a catalyst particle. However, his preliminary calculations suggested that this flow would be negligible except in the case of reactions at high pressure in catalysts with very large pores. It was only in 1974 that Komiyama and Inoue[3] realized the importance of intraparticle convection on the performance of a catalyst particle. They considered a first order reaction in an isothermal, finite cylinder lying parallel to the flow, and demonstrated both experimentally and theoretically that convection inside the particle increases significantly its effectiveness factor. Shortly after, Nir and Pismen[4] examined theoretically the effect of intraparticle convection for an irreversible, isothermal, first order reaction in slab, spherical, and cylindrical geometries. Here, the cylindrical pellet had infinite length and its axis lied perpendicular to the flow. For all three geometries, an appreciable enhancement of the catalyst effectiveness was observed in the parameter range where kinetics just becomes diffusion controlled. On the experimental side, the works of Cogan et al.[5] and Cresswell[6] should be mentioned. Cogan et al.[5] studied the depolymerization of paraldehyde, catalyzed by nickel sulfate supported on cylindrical pellets of porous silica gel, in a basket-type reactor. Those authors measured a significant increase of the effective reaction rate with the in-

Correspondence concerning this article should be addressed to S. S. S. Cardoso at Silvana_cardoso@cheng.cam.ac.uk.

tensity of the convective flux within the porous pellets. Creswell[6] presented a study of simultaneous intraparticle convection and diffusion in various α-alumina catalyst supports with bimodal and unimodal pore size distributions. He concluded that whilst the pore structure did not affect the effective diffusivity, it had a dramatic effect on permeability. The interaction of the external free fluid flow around a porous catalyst particle and the intraparticle flow field was analyzed by Stephanopoulos and Tsiveriotis.[7] They showed that transport outside the catalyst particle is unaffected by the intraparticle fluid flow and solved analytically the problem of convection, diffusion and zeroth-order reaction in spherical particle geometry. Later, Lu et al.[8] developed an analogy between the slab and sphere geometries for the problem of convection, diffusion and reaction in permeable isothermal particles with first order reaction. More recently, numerous publications have arisen considering the effects of intraparticle convection in chromatographic separations,[9–12] biological applications[13] and in the design of membrane reactors.[14,15] It should be noted that the contribution of intraparticle convection to the total mass transfer increases with the magnitude of the intraparticle mass Peclet number. In practice, significant mass Peclet numbers are achieved more easily in liquid systems than in gas phase reactions, due to the much higher chemical diffusivities in the latter. However, gaseous systems operating at high pressure[2] or involving diffusion in very large pore solids, such as in chromatographic applications,[9–12] can exhibit significant intraparticle convection.

Most of the aforementioned studies are concerned with isothermal conditions. However, many chemical and biochemical catalytic reactions have an appreciable heat of reaction. In this case, the overall performance of a catalyst particle depends not only on the concentration profile, but also on the temperature profile, inside the particle. Not surprisingly then, an important issue in the design and operation of catalytic reactors is the prediction of the maximum temperature inside the catalyst particles and its effect on the effectiveness factor. Rodrigues and Quinta Ferreira[16] addressed this gap in knowledge at the time and presented a numerical study of convective flow effects inside nonisothermal catalysts of slab geometry. Those authors also analyzed the effect of intraparticle convection on effective diffusivities inside large-pore supports. Lopes et al.[17] extended this work to consider in detail the flow field inside slab and spherical particle shapes. However, until now there has been no generalized theoretical analysis of the nonisothermal catalyst particle with simultaneous convection, diffusion, and reaction. The contribution of an analytical approach to this problem will thus be twofold. First, the analytical solutions will validate numerical results for extreme singular cases, such as those encountered when convective transport is much more important than diffusion in the particle. Secondly, analytical work will provide a framework to identify different regimes of operation of a catalyst particle and transitions between such regimes. The latter contribution is particularly important as a gateway to understanding the operation of actual catalytic pellets with nonsimple geometry and/or a complex intraparticle velocity field.

In the present article, we use a combination of perturbation and integral mathematical techniques to derive approximate analytical solutions for the concentration and temperature profiles, as well as the maximum temperature and the effectiveness factor, for a first order, nonisothermal reaction occurring in a catalyst slab. A comparison of our theoretical predictions with previous numerical simulations is presented.

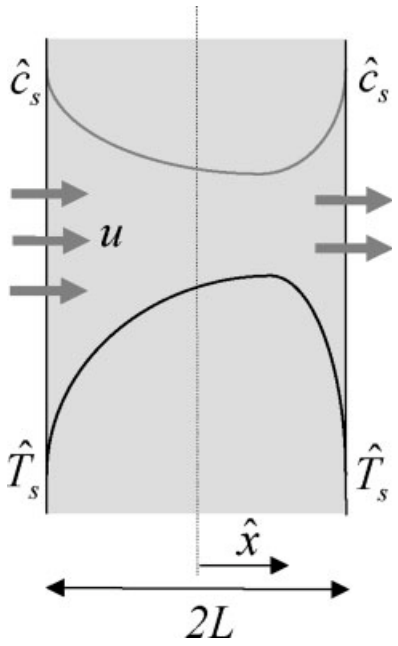

Figure 1. Catalyst slab, showing the asymmetric profiles of concentration of reactant A (gray curve) and of temperature (black curve) for an exothermic reaction.

Theory

Mass and energy balances

Consider a porous catalyst slab in which a first order chemical reaction A $\rightarrow$ B occurs, together with transport of heat and mass by convection and diffusion. The reaction is nonisothermal and irreversible. The two sides of the slab are maintained at uniform temperature and concentration of A, as shown in Figure 1. The transverse position within the slab is denoted by $\hat{x}$. The slab thickness, $2L$, is much smaller than its other dimensions, so that changes in temperature and concentration occur primarily in the $\hat{x}$-direction. Differential balances for mass of reactant A and energy are given, respectively, by

$$u\frac{d\hat{c}}{d\hat{x}} = D\frac{d^2\hat{c}}{d\hat{x}^2} - k\hat{c} \tag{1}$$

$$u\frac{d\hat{T}}{d\hat{x}} = \kappa\frac{d^2\hat{T}}{d\hat{x}^2} + \frac{qk}{\rho C_p}\hat{c} \tag{2}$$

with boundary conditions

$$\hat{c} = \hat{c}_s \text{ and } \hat{T} = \hat{T}_s \text{ at } \hat{x} = \pm L \tag{3a, b}$$

Here, $\hat{c}$ denotes the concentration of reactant A, $\hat{T}$ is temperature and the subscript s refers to surface conditions; k is the intrinsic kinetic constant, D is the effective coefficient of diffusion of A within the porous matrix of the catalyst and u is the superficial velocity of the fluid inside the slab, assumed to be constant. The density, specific heat and effective ther-

mal diffusivity of catalyst matrix filled with fluid are, respectively, ρ, C_p, and κ; these properties, which take into account contributions of both the solid and the fluid, are assumed to be constant. The heat of reaction is q. Some of the assumptions considered in the equations above merit discussion. In general, the flow field in the porous particle is driven by an external pressure gradient. Thus, the equations of continuity and momentum in the particle need to be solved simultaneously with those for conservation of reactant and energy. The numerical solution to this complex problem was considered by Lopes et al.[17] (1995). Those authors found that pressure-driven compressibility effects are negligible for values of $\beta = \Delta p/p_0$ up to 0.1; here Δp is the pressure change across the catalyst slab and p_0 is the pressure at the entrance to the slab. For values of $\beta_p \gg 0.1$, the effectiveness factor is lower than that predicted in the case of constant pressure, but the functional trends are the same. The analysis in the present paper, which assumes constant velocity across the catalyst slab and negligible compressibility effects, is therefore valid for $\beta_p < 0.1$. Additionally, in many practical conditions the external resistances to heat and mass transfer to/from the catalyst particle are important. In such cases, the temperature and concentration gradients around the catalyst particle are significant and the surface values are unknown. We shall see later, in the discussion section, how we can extend our results for prescribed surface temperature and concentration, to consider this more complex scenario.

To nondimensionalize Eqs. 1 and 2, we define dimensionless concentration, temperature and spatial position as follows:

$$c = \frac{\hat{c} - \hat{c}_s}{\hat{c}_s}, \quad T = \frac{\hat{T} - \hat{T}_s}{(\Delta\hat{T})_{ad}}, \quad x = \frac{\hat{x}}{L} \tag{4a - c}$$

where $(\Delta\hat{T})_{ad} = q\hat{c}_s/(\rho C_p)$ is the adiabatic temperature change, which would occur after complete reaction in a catalyst slab with initially uniform concentration of reactant $\hat{c}_s$ and no heat loss/gain at the surface. The Arrhenius temperature dependence of the rate constant k can be expressed in nondimensional form as

$$k = k_0 \exp\left(-\frac{E}{R\hat{T}}\right) = k_s \exp\left(\varphi \frac{T}{1+\eta T}\right) \tag{5}$$

Here, k_0 is a preexponential factor, k_s is the rate constant evaluated at the surface temperature of the catalyst,

$$\varphi = \frac{E(\Delta\hat{T})_{ad}}{R\hat{T}_s^2} \text{ and } \eta = \frac{(\Delta\hat{T})_{ad}}{\hat{T}_s}. \tag{6a, b}$$

Substituting Eqs. 4 and 5 into Eqs. 1–3 leads to the nondimensional mass and energy balances:

$$\frac{dc}{dx} = \frac{1}{Pe_m}\frac{d^2c}{dx^2} - \frac{\phi^2}{Pe_m} \exp\left(\varphi \frac{T}{1+\eta T}\right)(c+1) \tag{7}$$

$$\frac{dT}{dx} = \frac{1}{Pe_h}\frac{d^2T}{dx^2} + \frac{\phi^2}{Pe_m} \exp\left(\varphi \frac{T}{1+\eta T}\right)(c+1), \tag{8}$$

with boundary conditions

$$c = 0 \text{ and } T = 0 \text{ at } x = \pm 1 \tag{9a, b}$$

Here,

$$\phi = \left(\frac{k_s L^2}{D}\right)^{1/2} \tag{10}$$

is the Thiele modulus, and

$$Pe_m = \frac{uL}{D} \tag{11}$$

and

$$Pe_h = \frac{uL}{\kappa} \tag{12}$$

are the mass and heat Peclet numbers, respectively.

Inspection of Eqs. 7–9 suggests three different regimes of behavior for the catalyst slab: in regime I, characterized by small values of the Thiele modulus, the dominant phenomena are convection and diffusion; regime II is characterized by a large Thiele modulus, with diffusion and reaction being the dominant mechanisms; and finally, regime III occurs for intermediate values of the Thiele modulus, for which convection and reaction determine the catalyst behavior. We describe quantitatively each of these regimes of behavior in the next sections.

Regime I: diffusion and convection are dominant

We say the *Thiele modulus is small* when the three conditions

$$\frac{\phi^2}{Pe_m} \ll 1, \frac{1}{Pe_m}, \frac{1}{Pe_h} \tag{13}$$

are satisfied. When the Thiele modulus is small, chemical reaction is but a perturbation in a catalyst slab with simultaneous convection and diffusion of heat and mass. We can therefore conduct a perturbation analysis (see, e.g., Bender and Orszag[18]) and look for solutions of Eqs. 7–9 of the form

$$c(x) = \sum_{n=0}^{\infty} c_n(x)\varepsilon^n \tag{14}$$

$$T(x) = \sum_{n=0}^{\infty} T_n(x)\varepsilon^n \tag{15}$$

where $\varepsilon = \phi^2/Pe_m \ll 1$ is a small parameter, and $c_n(x)$ and $T_n(x)$ are perturbation functions of order n. Substituting Eqs. 14 and 15 into Eqs. 7 and 8 yields

$$\frac{d}{dx}\left[c_0 + c_1\varepsilon + c_2\varepsilon^2 + O(\varepsilon^3)\right] = \frac{1}{Pe_m}\frac{d^2}{dx^2}\left[c_0 + c_1\varepsilon + c_2\varepsilon^2 + O(\varepsilon^3)\right] - \varepsilon \exp\left\{\varphi \frac{T_0 + T_1\varepsilon + T_2\varepsilon^2 + O(\varepsilon^3)}{1+\eta\left[T_0 + T_1\varepsilon + T_2\varepsilon^2 + O(\varepsilon^3)\right]}\right\} \times \left[1 + c_0 + c_1\varepsilon + c_2\varepsilon^2 + O(\varepsilon^3)\right] \tag{16}$$

$$\frac{d}{dx}\left[T_0 + T_1\varepsilon + T_2\varepsilon^2 + O(\varepsilon^3)\right] = \frac{1}{Pe_h}\frac{d^2}{dx^2}\left[T_0 + T_1\varepsilon + T_2\varepsilon^2 + O(\varepsilon^3)\right] + \varepsilon \exp\left\{\varphi \frac{T_0 + T_1\varepsilon + T_2\varepsilon^2 + O(\varepsilon^3)}{1+\eta\left[T_0 + T_1\varepsilon + T_2\varepsilon^2 + O(\varepsilon^3)\right]}\right\} \times \left[1 + c_0 + c_1\varepsilon + c_2\varepsilon^2 + O(\varepsilon^3)\right] \tag{17}$$

The boundary conditions are expanded in a similar manner to give

$$\begin{aligned} c_0 + c_1\varepsilon + c_2\varepsilon^2 + O(\varepsilon^3) &= 0 \\ T_0 + T_1\varepsilon + T_2\varepsilon^2 + O(\varepsilon^3) &= 0 \end{aligned} \quad \text{at } x = \pm 1 \qquad (18a, b)$$

When the coefficients of successive powers of ε are separately equated to zero, an infinite set of differential equations and a sufficient set of boundary conditions are obtained. The $O(1)$ problem is the same as setting $\varepsilon = 0$ in the original equations, i.e., a diffusive and convective system with no reaction, and has solution

$$\begin{aligned} c_0 &= 0 \\ T_0 &= 0 \end{aligned} \qquad (19a, b)$$

The $O(\varepsilon)$ problem yields the perturbation functions

$$\begin{aligned} c_1 &= \frac{2e^{Pe_m(1+x)}}{-1+e^{2Pe_m}} - \frac{1+e^{2Pe_m}}{-1+e^{2Pe_m}} - x \\ T_1 &= \frac{2e^{Pe_h(1+x)}}{-1+e^{2Pe_h}} + \frac{1+e^{2Pe_h}}{-1+e^{2Pe_h}} + x \end{aligned} \qquad (20a, b)$$

Thus, the two-term expansions for $c(x)$ and $T(x)$ are

$$\begin{aligned} c(x) &= \frac{\phi^2}{Pe_m}\left[\frac{2e^{Pe_m(1+x)}}{-1+e^{2Pe_m}} - \frac{1+e^{2Pe_m}}{-1+e^{2Pe_m}} - x\right] + O\left(\frac{\phi^4}{Pe_m^2}\right) \\ T(x) &= \frac{\phi^2}{Pe_m}\left[-\frac{2e^{Pe_h(1+x)}}{-1+e^{2Pe_h}} + \frac{1+e^{2Pe_h}}{-1+e^{2Pe_h}} + x\right] + O\left(\frac{\phi^4}{Pe_m^2}\right) \end{aligned} \qquad (21a, b)$$

In the diffusive limit Pe_m, $Pe_h \to 0$, i.e. when convection becomes negligible compared to diffusion, solutions 21 reduce to previously known perturbation solutions for a system with only diffusion and reaction.[19]

For an exothermic reaction the maximum temperature and the minimum concentration occur at

$$x_{max} = -1 + \frac{1}{Pe_h}\ln\left(-\frac{1-e^{2Pe_h}}{2Pe_h}\right) \qquad (22)$$

The maximum temperature is hence given by

$$\begin{aligned} T_{max} = T(x_{max}) = \frac{\phi^2}{Pe_m}\Bigg[&\frac{2}{-1+e^{2Pe_h}} + \frac{1-e^{2Pe_h}}{(-1+e^{2Pe_h})Pe_h} \\ &+ \frac{1}{Pe_h}\ln\left(-\frac{1-e^{2Pe_h}}{2Pe_h}\right)\Bigg] + O\left(\frac{\phi^4}{Pe_m^2}\right) \end{aligned} \qquad (23)$$

In the limit $Pe_h \to 0$, i.e. for a highly conductive catalyst material,

$$T_{max} \to \frac{\phi^2}{Pe_m}\left(\frac{Pe_h}{2} - \frac{Pe_h^3}{36}\right) + O\left(\frac{\phi^4}{Pe_m^2}\right) \qquad (24)$$

which is consistent with previously known results for a diffusive and reactive system without convection.[19] And, finally, in the limit $Pe_h \to \infty$, i.e. for a poorly conductive catalyst,

$$T_{max} \to \frac{\phi^2}{Pe_m}\left(2 - \frac{1}{Pe_h}\right) + O\left(\frac{\phi^4}{Pe_m^2}\right) \qquad (25)$$

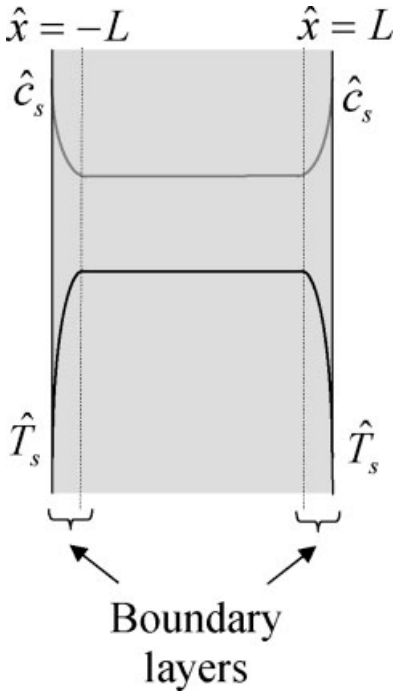

Figure 2. Catalyst slab, showing the concentration and thermal boundary layers that develop at the entrance and exit of the slab for regime II, when diffusion and reaction are dominant ($\phi^2/Pe_m \gg 1$, $1/Pe_h$, $1/Pe_m$).

Regime II: diffusion and reaction are dominant

We say the *Thiele modulus is large* when the three conditions

$$\frac{\phi^2}{Pe_m} \gg 1, \frac{1}{Pe_m}, \frac{1}{Pe_h} \qquad (26)$$

are satisfied. When the Thiele modulus is large, the chemical reaction is fast and leads to a sharp decline in concentration near the surface of the catalyst slab. Similarly, there is a sharp change in temperature near the edges of the slab: an increase for exothermic and decrease for endothermic reactions. Thus, concentration and thermal boundary layers develop at $\hat{x} = \pm L$, as shown in Figure 2. In this limit, we conduct a singular perturbation analysis and look for solutions of Eqs. 7–9 of the form

$$c(x) = \sum_{n=0}^{\infty} c_n(x)\varepsilon^{n/2} \qquad (27)$$

$$T(x) = \sum_{n=0}^{\infty} T_n(x)\varepsilon^{n/2} \qquad (28)$$

where $\varepsilon = Pe_m/\phi^2 \ll 1$ is a small parameter, and $c_n(x)$ and $T_n(x)$ are perturbation functions of order n.

Middle Region. Let us consider first the region of the catalyst slab away from the boundary layers, i.e., the middle region (Figure 2). The concentration and temperature in this

region are denoted by $c^m(x)$ and $T^m(x)$, respectively. After substituting Eqs. 27 and 28 into Eqs. 7–9, we simply collect terms of similar order with respect to the small parameter $\varepsilon = Pe_m/\phi^2$. Solution of the $O(1)$ problem gives

$$c_0^m = -1 \tag{29}$$

and no information is gained about ${T_0}^m(x)$. At $O(\varepsilon^{1/2})$, we find

$$c_1^m = 0 \tag{30}$$

and at $O(\varepsilon)$ we have

$$c_2^m = 0$$
$$T_0^m = A_1 + \frac{A_2}{Pe_h} e^{Pe_h x} \tag{31a,b}$$

where A_1 and A_2 are constants to be determined. Finally, at $O(\varepsilon^{3/2})$ we get

$$c_3^m = 0$$
$$T_1^m = A_3 + \frac{A_4}{Pe_h} e^{Pe_h x} \tag{32a,b}$$

where A_3 and A_4 are also constants to be determined.

Region near $x = 1$. In the boundary layer near $x = 1$, the stretching transformation

$$X = (1-x)\varepsilon^{-1/2} \tag{33}$$

is applied, after which $c^{rb}(X)$ and $T^{rb}(X)$ are expanded in a power series in $\varepsilon^{1/2} = \sqrt{Pe_m}/\phi$. Solution of the $O(1)$, for small $\varphi Pe_h/Pe_m$ and $\eta Pe_h/Pe_m$, yields

$$c_0^{rb} = -1 + e^{-b\sqrt{Pe_m}X}$$
$$T_0^{rb} = \frac{Pe_h}{Pe_m}\left[1 - e^{-b\sqrt{Pe_m}X}\right] \tag{34a,b}$$

where

$$b = \left(\frac{e^{\varphi Pe_h/Pe_m} - 1}{\varphi Pe_h/Pe_m}\right)^{1/2} \tag{35}$$

A detailed derivation of the solution above is given in Appendix.

At $O(\varepsilon^{1/2})$ and after appropriate matching of the middle and right boundary layer solutions, we find

$$c_1^{rb} = \frac{b\sqrt{Pe_m}}{b^2-d}\left(e^{-b\sqrt{Pe_m}X} - e^{-\sqrt{d}\sqrt{Pe_m}X}\right)$$
$$T_1^{rb} = -\frac{Pe_h}{\sqrt{Pe_m}}\frac{b}{b^2-d}\left(e^{-b\sqrt{Pe_m}X} - e^{-\sqrt{d}\sqrt{Pe_m}X}\right)$$
$$+ \frac{Pe_h}{b\sqrt{Pe_m}}\left(e^{-b\sqrt{Pe_m}X} - 1\right)\left(1 - \frac{Pe_h}{Pe_m}\right) \tag{36a,b}$$

where

$$d = e^{\varphi Pe_h/Pe_m} \tag{37}$$

Region near $x = -1$. In the left-hand-side boundary layer, near $x = -1$, we apply the stretching transformation

$$Y = (1+x)\varepsilon^{-1/2} \tag{38}$$

Following a solution procedure similar to that for the right boundary layer, we find at $O(1)$,

$$c_0^{lb} = -1 + e^{-b\sqrt{Pe_m}Y}$$
$$T_0^{lb} = \frac{Pe_h}{Pe_m}\left[1 - e^{-b\sqrt{Pe_m}Y}\right] \tag{39a,b}$$

And at $O(\varepsilon^{1/2})$,

$$c_1^{lb} = \frac{b\sqrt{Pe_m}}{b^2-d}\left(-e^{-b\sqrt{Pe_m}Y} + e^{-\sqrt{d}\sqrt{Pe_m}Y}\right)$$
$$T_1^{lb} = -\frac{Pe_h}{\sqrt{Pe_m}}\frac{b}{b^2-d}\left(e^{-b\sqrt{Pe_m}Y} + e^{-\sqrt{d}\sqrt{Pe_m}Y}\right)$$
$$-\frac{Pe_h}{b\sqrt{Pe_m}}\left(e^{-b\sqrt{Pe_m}Y} - 1\right)\left(1 - \frac{Pe_h}{Pe_m}\right) \tag{40a,b}$$

Composite Solution. The final composite solution, valid across the whole of the catalyst width, is given by

$$c = c^{lb} + c^m + c^{rb} - \lim_{Y\to\infty} c^{lb} - \lim_{X\to\infty} c^{rb}$$
$$T = T^{lb} + T^m + T^{rb} - \lim_{Y\to\infty} T^{lb} - \lim_{X\to\infty} T^{rb} \tag{41a,b}$$

Matching of the solutions for the left boundary layer, middle region and right boundary layer of the slab allow us to determine the constants A_1 through to A_4 in Eqs. 31 and 32, leading to the solutions

$$T_0^m = \frac{Pe_h}{Pe_m} \tag{42}$$

$$T_1^m = -\frac{2}{b\sqrt{Pe_m}}\left(1 - \frac{Pe_h}{Pe_m}\right)\frac{Pe_h}{e^{Pe_h} - e^{Pe_h}}\left(-\frac{e^{Pe_h} + e^{-Pe_h}}{2} + e^{Pe_h x}\right) \tag{43}$$

Equation 41 then yields

$$c(x) = -1 + e^{-b(1-x)\phi} + e^{-b(1+x)\phi} + \frac{bPe_m}{(b^2-d)\phi}$$
$$\times\left[e^{-b(1-x)\phi} - e^{-\sqrt{d}(1-x)\phi} - e^{-b(1+x)\phi} + e^{-\sqrt{d}(1+x)\phi}\right] + O\left(\frac{Pe_m}{\phi^2}\right)$$
$$T(x) = \frac{Pe_h}{Pe_m}\left\{1 - \frac{2Pe_m}{b\phi}\left(1 - \frac{Pe_h}{Pe_m}\right)\frac{1}{e^{Pe_h} - e^{-Pe_h}}\right.$$
$$\times\left(-\frac{e^{Pe_h} + e^{Pe_h}}{2} + e^{Pe_h x}\right) - e^{-b(1-x)\phi} - e^{-b(1+x)\phi} - \frac{bPe_m}{(b^2-d)\phi}$$
$$\times\left[e^{-b(1-x)\phi} - e^{-\sqrt{d}(1-x)\phi} - e^{-b(1+x)\phi} + e^{-\sqrt{d}(1+x)\phi}\right] + \frac{Pe_m}{b\phi}$$
$$\left.\times\left(1 - \frac{Pe_h}{Pe_m}\right)\left[e^{-b(1-x)\phi} - e^{-b(1+x)\phi}\right]\right\} + O\left(\frac{Pe_m}{\phi^2}\right) \tag{44a,b}$$

We may show that for large Thiele modulus the maximum temperature is given by

$$T_{max} = \frac{Pe_h}{Pe_m}\left(1 + \frac{Pe_m}{b\phi}\left|1 - \frac{Pe_h}{Pe_m}\right|\right) + O\left(\frac{Pe_m}{\phi^2}\right) \tag{45a,b}$$

for an exothermic reaction.

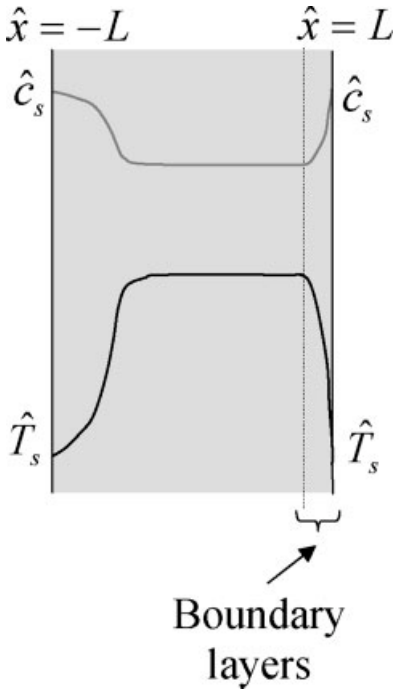

Figure 3. Catalyst slab, showing the concentration and thermal boundary layers that develop only at the exit of the slab for regime III, when convection and reaction are dominant (ϕ^2/Pe_m ~1, and $1/Pe_h$, $1/Pe_m \gg 1$).

We note that at $O(1)$ solutions 44 and 45 coincide with those previously presented for a diffusive and reactive system[19] without convection. The effect of convection arises at $O(\varepsilon^{1/2}) = O(\sqrt{Pe_m}/\phi)$.

Regime III: convection and reaction are dominant

We say the *Thiele modulus is of intermediate value* when the three conditions

$$\frac{\phi^2}{Pe_m} \sim 1 \quad \text{and} \quad \frac{1}{Pe_h}, \frac{1}{Pe_m} \ll 1 \tag{46}$$

are satisfied. When the Thiele modulus is intermediate, the chemical reaction is fast and leads to a sharp decline in concentration near the exit of the catalyst slab. Similarly, there is a sharp change in temperature near the exit of the slab: an increase for exothermic and decrease for endothermic reactions. Thus, concentration and thermal boundary layers develop at $\hat{x} = L$ for a flow from left to right, as shown in Figure 3. In this limit, we conduct a singular perturbation analysis and look for solutions of Eqs. 7–9 of the form

$$c(x) = \sum_{n=0}^{\infty} c_n(x)\varepsilon^n \tag{47}$$

$$T(x) = \sum_{n=0}^{\infty} T_n(x)\varepsilon^n \tag{48}$$

where $\varepsilon = 1/Pe_m \ll 1$ is a small parameter, and $c_n(x)$ and $T_n(x)$ are perturbation functions of order n.

Left and Middle Region. In the region of the catalyst slab away from the boundary layer, i.e., in the left and middle region (Figure 3), we solve Eqs. 7–9 with expansions 47 and 48. We denote the concentration and temperature in this region by $c^{lm}(x)$ and $T^{lm}(x)$, respectively. Solution of the $O(1)$ problem gives the implicit profiles

$$e^{-\varphi}\left\{Ei[\varphi(1+c_0^{lm}) - Ei(\varphi)]\right\} = -\frac{\phi^2}{Pe_m}(x+1)$$
$$T_0^{lm} = -c_0^{lm} \tag{49a, b}$$

where Ei denotes the exponential integral function. In this regime it is difficult to calculate the second order terms, so we shall derive perturbation expansions with one term only.

Region near $x = 1$. In the boundary layer near $x = 1$, the stretching transformation

$$X = (1-x)\varepsilon^{-1} \tag{50}$$

is applied. We then solve Eqs. 7–9 with this transformation and expansions 47 and 48. At $O(1)$, the solutions are

$$c_0^{rb} = a(1 - e^{-X})$$
$$T_0^{rb} = -a(1 - e^{-Pe_h X/Pe_m}) \tag{51a, b}$$

where a is a constant to be determined.

Matching the middle and right boundary layer solutions, we find

$$a = -1 + \frac{1}{\varphi} Ei^{-1}\left\{Ei(\varphi) - 2e^{\varphi}\frac{\phi^2}{Pe_m}\right\} \tag{52}$$

Composite Solution. The final composite solution, valid across the whole of the catalyst width, is given by

$$c = c^{lm} + c^{rb} - \lim_{X\to\infty} c^{rb}$$
$$T = T^{lm} + T^{rb} - \lim_{X\to\infty} T^{rb} \tag{53a, b}$$

yielding

$$c(x) = -1 + \frac{1}{\varphi} Ei^{-1}\left\{Ei(\varphi) - (x+1)e^{\varphi}\frac{\phi^2}{Pe_m}\right\} - ae^{-(1-x)Pe_m} + O\left(\frac{1}{Pe_m}\right)$$
$$T(x) = 1 - \frac{1}{\varphi} Ei^{-1}\left\{Ei(\varphi) - (x+1)e^{\varphi}\frac{\phi^2}{Pe_m}\right\} + ae^{-(1-x)Pe_h} + O\left(\frac{1}{Pe_m}\right) \tag{54a, b}$$

These solutions show that even when convection and reaction dominate, diffusion of reactant A and conduction of heat still play a role at $O(1)$, albeit only in thin boundary layers at the exit of the catalyst slab.

For an exothermic reaction, the maximum temperature is given by

$$T_{max} = -a + O\left(\frac{1}{Pe_m}\right) \tag{55}$$

We note that a depends on the Thiele modulus ϕ through Eq. 52 and we do not know a priori the value of ϕ at

which the temperature is maximum. However, for large φ we may make the $\sim a = -1$ and relation (55) simplifies to

$$T_{\max} = -1 + O\left(\frac{1}{Pe_{\mathrm{m}}}\right) \tag{56}$$

The effectiveness factor

The overall performance of a catalyst slab is measured by its effectiveness factor,

$$\mathrm{Eff} = \frac{\int_{-L}^{+L} k\hat{c}\, d\hat{x}}{\int_{-L}^{+L} k_{\mathrm{s}}\, \hat{c}_{\mathrm{s}}\, d\hat{x}}, \tag{57}$$

which compares the average reaction rate to the reaction rate that would be observed if the concentration of reactant and temperature throughout the slab were equal to those at the surface. Using Gauss' divergence theorem, it may be shown that in terms of our nondimensional variables,

$$\mathrm{Eff} = \frac{1}{2\phi^2}\left(\left.\frac{dc}{dx}\right|_{x=1} - \left.\frac{dc}{dx}\right|_{x=-1}\right) \tag{58}$$

It is now very easy to determine the effectiveness factor in the limits of small and large Thiele modulus. Using our results 21, 44, and 54 in Eq. 58 gives,

for regime I,

$$\mathrm{Eff} = 1 + \phi^2\left\{-\frac{\varphi}{Pe_{\mathrm{m}}Pe_{\mathrm{h}}} + \frac{(1+e^{2Pe_{\mathrm{h}}})\varphi}{(-1+e^{2Pe_{\mathrm{h}}})Pe_{\mathrm{m}}} - \frac{1+e^{2Pe_{\mathrm{m}}}(-1+Pe_{\mathrm{m}})+Pe_{\mathrm{m}}}{(-1+e^{2Pe_{\mathrm{m}}})Pe_{\mathrm{m}}^2}\right\} + O\left(\frac{\phi^4}{Pe_{\mathrm{m}}^3}\right) \tag{59}$$

for regime II,

$$\mathrm{Eff} = \frac{b}{\phi} + \frac{b^3 + bd - 2b^2\, d^{1/2}}{2(b^2-d)^2}\frac{Pe_{\mathrm{m}}^2}{\phi^3} + O\left(\frac{Pe_{\mathrm{m}}^{3/2}}{\phi^5}\right) \tag{60}$$

and for regime III,

$$\mathrm{Eff} = \frac{1}{2\phi^2}\left[-aPe_{\mathrm{m}} + \frac{\phi^2}{Pe_{\mathrm{m}}}\right] + O\left(\frac{1}{\phi^2 Pe_{\mathrm{m}}}\right) \tag{61}$$

We note that in the calculation of Eqs. 59 and 60, we used a third term in solutions 21 and 44. We do not present these extra terms in the paper because they are extremely long and have been used only in the intermediate calculation of the effectiveness factor.

Table 1. Perturbation Solutions for the Effectiveness Factor, Maximum Temperature, and the Concentration and Temperature Profiles Inside a Catalyst Slab for a First Order Chemical Reaction

Regime I: diffusion and convection dominant $\left(\frac{\phi^2}{Pe_{\mathrm{m}}} \ll 1,\ \frac{1}{Pe_{\mathrm{h}}},\ \frac{1}{Pe_{\mathrm{m}}}\right)$

$$\mathrm{Eff} = 1 + \phi^2\left\{-\frac{\gamma\beta}{Pe_{\mathrm{h}}^2} + \frac{(1+e^{2Pe_{\mathrm{h}}})\gamma\beta}{(-1+e^{2Pe_{\mathrm{h}}})Pe_{\mathrm{h}}} - \frac{1+e^{2Pe_{\mathrm{m}}}(-1+Pe_{\mathrm{m}})+Pe_{\mathrm{m}}}{(-1+e^{2Pe_{\mathrm{m}}})Pe_{\mathrm{m}}^2}\right\} \tag{62}$$

$$\frac{\hat{T}_{\max}}{\hat{T}_{\mathrm{s}}} = 1 + \beta\frac{\phi^2}{Pe_{\mathrm{h}}}\left\{\frac{2}{-1+e^{2Pe_{\mathrm{h}}}} + \frac{1-e^{2Pe_{\mathrm{h}}}}{(-1+e^{2Pe_{\mathrm{h}}})Pe_{\mathrm{h}}} + \frac{1}{Pe_{\mathrm{h}}}\ln\left(-\frac{1-e^{2Pe_{\mathrm{h}}}}{2Pe_{\mathrm{h}}}\right)\right\} \tag{63}$$

$$\frac{\hat{c}}{\hat{c}_{\mathrm{s}}} = 1 + \frac{\phi^2}{Pe_{\mathrm{m}}}\left[\frac{2e^{Pe_{\mathrm{m}}(1+x)}}{-1+e^{2Pe_{\mathrm{m}}}} - \frac{1+e^{2Pe_{\mathrm{m}}}}{-1+e^{2Pe_{\mathrm{m}}}} - x\right] \tag{64}$$

$$\frac{\hat{T}}{\hat{T}_{\mathrm{s}}} = 1 + \beta\frac{\phi^2}{Pe_{\mathrm{h}}}\left[-\frac{2e^{Pe_{\mathrm{h}}(1+x)}}{-1+e^{2Pe_{\mathrm{h}}}} + \frac{1+e^{2Pe_{\mathrm{h}}}}{-1+e^{2Pe_{\mathrm{h}}}} + x\right] \tag{65}$$

Regime II: diffusion and reaction dominant $\left(\frac{\phi^2}{Pe_{\mathrm{m}}} \gg 1,\ \frac{1}{Pe_{\mathrm{h}}},\ \frac{1}{Pe_{\mathrm{m}}}\right)$

$$\mathrm{Eff} = \frac{b}{\phi} + \frac{b^3 + bd - 2b^2 d^{1/2}}{2(b^2-d)^2}\frac{Pe_{\mathrm{m}}^2}{\phi^3} \tag{66}$$

$$\frac{\hat{T}_{\max}}{\hat{T}_{\mathrm{s}}} = 1 + \beta\left(1 + \frac{Pe_{\mathrm{m}}}{b\phi}\left|1 - \frac{Pe_{\mathrm{h}}}{Pe_{\mathrm{m}}}\right|\right) \tag{67}$$

$$\frac{\hat{c}}{\hat{c}_{\mathrm{s}}} = e^{-b(1-x)\phi} + e^{-b(1+x)\phi} + \frac{bPe_{\mathrm{m}}}{(b^2-d)\phi}\left[e^{-b(1-x)\phi} - e^{-\sqrt{d}(1-x)\phi} - e^{-b(1+x)\phi} + e^{-\sqrt{d}(1+x)\phi}\right] \tag{68}$$

$$\frac{\hat{T}}{\hat{T}_{\mathrm{s}}} = 1 + \beta\left\{1 - \frac{2Pe_{\mathrm{m}}}{b\phi}\left(1 - \frac{Pe_{\mathrm{h}}}{Pe_{\mathrm{m}}}\right)\frac{1}{e^{Pe_{\mathrm{h}}} - e^{-Pe_{\mathrm{h}}}}\left(-\frac{e^{Pe_{\mathrm{h}}} + e^{-Pe_{\mathrm{h}}}}{2} + e^{Pe_{\mathrm{h}}x}\right) - e^{-b(1-x)\phi} - e^{-b(1+x)\phi}\right.$$
$$\left. - \frac{bPe_{\mathrm{m}}}{(b^2-d)\phi}\left[e^{-b(1-x)\phi} - e^{-\sqrt{d}(1-x)\phi} - e^{-b(1+x)\phi} + e^{-\sqrt{d}(1+x)\phi}\right] + \frac{Pe_{\mathrm{m}}}{b\phi}\left(1 - \frac{Pe_{\mathrm{h}}}{Pe_{\mathrm{m}}}\right)\left[e^{-b(1-x)\phi} - e^{-b(1+x)\phi}\right]\right\} \tag{69}$$

Table 1. *continued*

Regime III: convection and reaction dominant ($\frac{\phi^2}{Pe_m} \sim 1$ and $\frac{1}{Pe_h}, \frac{1}{Pe_m} \ll 1$)

$$\text{Eff} = \frac{1}{2\phi^2}\left[-aPe_m + \frac{\phi^2}{Pe_m}\right] \tag{70}$$

$$\frac{\hat{T}_{max}}{\hat{T}_s} \approx 1 + \beta\frac{Pe_m}{Pe_h} = 1 + \frac{q\hat{c}_s}{\rho C_p \hat{T}_s} \text{ for } Pe_m \gg (1/\gamma\beta)Pe_h \tag{71}$$

$$\frac{\hat{c}}{\hat{c}_s} = \frac{1}{\gamma\beta Pe_m/Pe_h} Ei^{-1}\left\{Ei(\gamma\beta Pe_m/Pe_h) - (x+1)e^{\gamma\beta Pe_m/Pe_h}\frac{\phi^2}{Pe_m}\right\} - ae^{-(1-x)Pe_m} \tag{72}$$

$$\frac{\hat{T}}{\hat{T}_s} = 1 + \beta\frac{Pe_m}{Pe_h}\left[1 - \frac{1}{\gamma\beta Pe_m/Pe_h} Ei^{-1}\left\{Ei(\gamma\beta Pe_m/Pe_h) - (x+1)e^{\gamma\beta Pe_m/Pe_h}\frac{\phi^2}{Pe_m}\right\} + ae^{-(1-x)Pe_h}\right] \tag{73}$$

where

$$a = -1 + \frac{1}{\gamma\beta Pe_m/Pe_h} Ei^{-1}\left\{Ei(\gamma\beta Pe_m/Pe_h) - 2e^{\gamma\beta Pe_m/Pe_h}\frac{\phi^2}{Pe_m}\right\} \tag{74}$$

$$b = \left(\frac{e^{\gamma\beta}-1}{\gamma\beta}\right)^{1/2} \tag{75}$$

$$d = e^{\gamma\beta} \tag{76}$$

Discussion

The analytical solutions derived in the previous section allow the determination of the concentration and temperature profiles, as well as the effectiveness factor and transport rates, for a variety of operating conditions and particle characteristics. In this section, the behavior of our solutions in the isothermal limit is examined and a comparison with previous numerical data is presented.

The main results of the previous section may be expressed in terms of the well-known Prater $\beta = q\hat{c}_s D/(\rho C_p \hat{T}_s \kappa)$ and Arrhenius $\gamma = E/(R\hat{T}_s)$ numbers. Indeed, we note that $\varphi Pe_h/Pe_m = \gamma\beta$ and $\eta Pe_h/Pe_m = \beta$. Table 1 summarizes our results for the concentration and temperature profiles, as well as the maximum temperature and effectiveness factor, in terms of β and γ.

We begin by looking at the behavior of our solutions in the isothermal limit, i.e., when $\beta \to 0$. In this limit, $b \to 1$, $d \to 1$, $a \to -1 + e^{-2\phi^2/Pe_m}$ [see Eqs. 74–76] and the effectiveness factor is given by:

for regime I, when diffusion and convection dominate ($\phi^2/Pe_m \ll 1$, $1/Pe_h$, $1/Pe_m$)

$$\text{Eff} = 1 + \frac{\phi^2}{Pe_m}[1 - Pe_m \coth(Pe_m)] + O\left(\frac{\phi^4}{Pe_m^3}\right) \tag{77}$$

for regime II, when diffusion and reaction dominate ($\phi^2/Pe_m \gg 1$, $1/Pe_h$, $1/Pe_m$),

$$\text{Eff} = \frac{1}{\phi} + \frac{1}{8}\frac{Pe_m^2}{\phi^3} + O\left(\frac{Pe_m^{3/2}}{\phi^5}\right) \tag{78}$$

and for regime III, when convection and reaction dominate ($\phi^2/Pe_m \sim 1$, and $1/Pe_h$, $1/Pe_m \ll 1$),

$$\text{Eff} = \frac{1}{2\phi^2}\left[\left(1 - e^{-2\phi^2/Pe_m}\right)Pe_m + \frac{\phi^2}{Pe_m}\right] + O\left(\frac{1}{\phi^2 Pe_m}\right) \tag{79}$$

It may be shown that relations Eqs. 77 and 78 agree with the results of Nir and Pismen[4] for convection, diffusion and reaction in an isothermal slab when we consider the limits of slow and fast reaction, respectively. A comparison of our prediction for regime III, given in Eq. 79, with the results of those authors are more difficult. However, a perturbation analysis of the isothermal problem in this convective limit gives the concentration profile

$$c(x) = (1 - e^{-2\phi^2/Pe_m}) + e^{-(1-x)Pe_m}(1 - e^{-2\phi^2/Pe_m}) + O\left(\frac{1}{\phi^2 Pe_m}\right) \tag{80}$$

from which the effectiveness factor may be calculated using Eq. 58. The result obtained in this way agrees with expression 79. Our results for the nonisothermal convective problem are therefore consistent with well-known results in the isothermal limit.

To test directly the accuracy of our approximate perturbation solutions, we compare their predictions with the results obtained from numerical integration of the governing equations. We shall use for this the numerical results reported by Quinta Ferreira[20] for a catalyst slab undergoing a first order, nonisothermal reaction because these were readily available in a convenient format. Figures 4 and 5 show a comparison between these numerical results and our analytical predictions for the concentration and temperature profiles. The agreement is very good. For small Thiele modulus, when diffusion and convection dominate (regime I), our regular perturbation solutions overlap with the numerical results. For large Thiele modulus, when diffusion and reaction dominate (regime II), our singular perturbation predictions are close to the numerical solution; we recall that our results here involved an approximate solution of a nonlinear perturbation problem at $O(1)$, so the agreement is rather good. For intermediate values of the Thiele modulus, when convection and reaction dominate (regime III), the agreement is not as striking as in the other regimes but is still acceptable, particularly if we note that

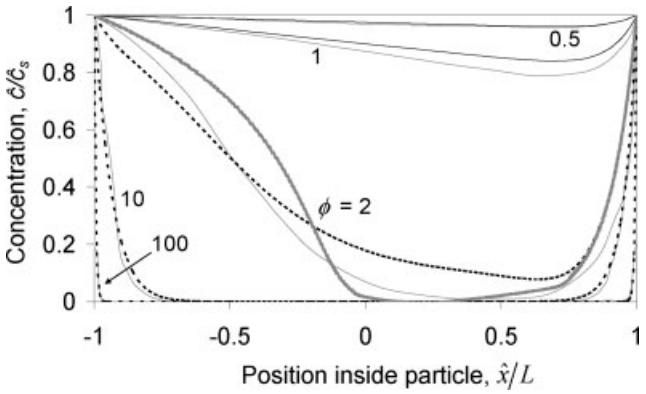

Figure 4. Reactant concentration profile inside a catalyst slab for a first-order chemical reaction.

Shown are the numerical results of Quinta Ferreira (1988, grey lines), the regular perturbation predictions for low Thiele modulus (solid black lines), the singular perturbation predictions for high Thiele modulus (dashed black lines) and the singular perturbation predictions for intermediate values of the Thiele modulus (thick grey line), for $\gamma = 20$, $\beta = 0.1$, $Pe_h = 5$ and $Pe_m = 10$.

in this case we are using a one-term only perturbation solution.

Figure 6 shows a comparison between the numerical results of Quinta Ferreira[20] and our analytical predictions for the maximum temperature as a function of mass Peclet number, for regime III. There is excellent agreement for $Pe_h = 5$ and $Pe_h = 25$. For $Pe_h = 10$, there is some deviation, which we believe might be due to difficulties with the numerical integration; indeed, for all runs in this regime, the conservation equations are difficult to integrate numerically because of the low magnitude of the coefficient of the highest order derivative. We also note that our prediction in Eqs. 56 or 71 is valid only for large φ, which is equivalent to $Pe_m \gg (1/\gamma\beta)Pe_h$ (see Table 1). This assumption is not too restrictive in practice given that, for gaseous streams undergoing reaction in porous solid catalysts, $Pe_m/Pe_h \sim 10 - 10^4$, and for liquid streams $Pe_m/Pe_h \sim 50 - 10^3$ (see e.g. Satterfield[21] and Rodrigues et al.[22]). Figure 6 and Eq. 71 might be misleading in that it appears that the maximum temperature is a function of the ratio of the Peclet numbers. However, interestingly, a careful look at Eq. 71 shows that the maximum temperature change achieved inside a catalyst slab is simply $(\Delta\hat{T})_{ad} = q^{\hat{c}_s}/(\rho C_p)$, i.e., the adiabatic temperature change, which would occur after complete reaction in a catalyst slab with initially uniform concentration of reactant $\hat{c}_s$ and no heat loss/gain at the surface. This means that, to leading order, the maximum temperature is independent of the mass and heat Peclet numbers in regime III.

The variation of the effectiveness factor with the Thiele modulus is shown in Figure 7, for a selection of mass Peclet numbers. For intermediate values of the Thiele modulus, the effectiveness factor is multi-valued, exhibiting three steady states. The lower branch corresponds to a low temperature, stable solution in which the catalyst particle is nonignited and the effectiveness factor is close to 1; the intermediate branch is an unstable solution; and the upper branch is a high temperature, stable solution in which the catalyst is ignited. We present here analytical results for only the stable solutions in this region. The full numerical results and approximate analytical predictions are in excellent agreement for regimes I, II, and III. We see that the maximum effectiveness factor is obtained in regime III, i.e., when convection and reaction are dominant, with diffusion being important only in the thermal and concentration boundary layers at the exit of the catalyst slab ($x = L$). Figure 7 and Eq. 70 show that, to leading order, the maximum effectiveness factor is approximately proportional to the mass Peclet number and is independent of the heat Peclet number.

In this article, we presented results for only $\gamma = 20$. However, the solutions for regime II assumed both $\eta Pe_h/Pe_m = \beta$ and $\varphi Pe_h/Pe_m = \gamma\beta$ to be small. In general, we expect good

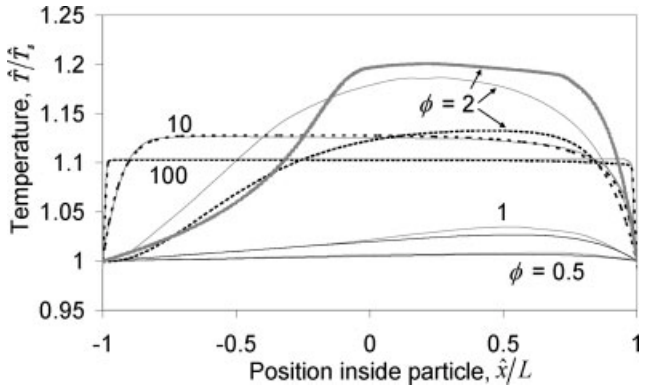

Figure 5. Temperature profile inside a catalyst slab for a first-order chemical reaction.

Shown are the numerical results of Quinta Ferreira (1988, grey lines), the regular perturbation predictions for low Thiele modulus (solid black lines), the singular perturbation predictions for high Thiele modulus (dashed black lines) and the singular perturbation predictions for intermediate values of the Thiele modulus (thick grey line), for $\gamma = 20$, $\beta = 0.1$, $Pe_h = 5$ and $Pe_m = 10$.

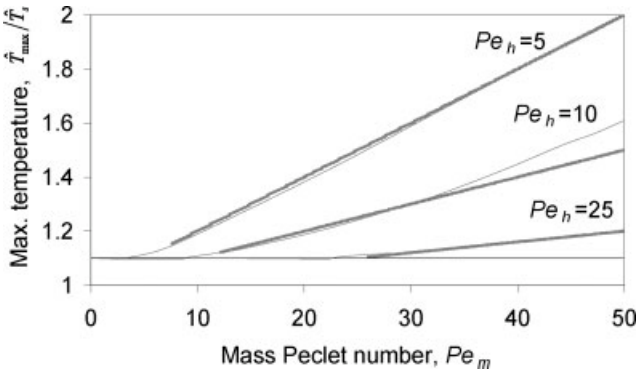

Figure 6. Maximum temperature inside a catalyst slab for a first-order chemical reaction.

Shown are the numerical results of Quinta Ferreira (1988, grey lines) and the singular perturbation predictions for intermediate values of the Thiele modulus (thick grey lines), for $\gamma = 20$ and $\beta = 0.1$. Note that in the limit of $Pe_m \to 0$, the maximum temperature tends to the well-known diffusive limit $\hat{T}_{max} \to \hat{T}_s(1 + \beta)$ (solid black line).

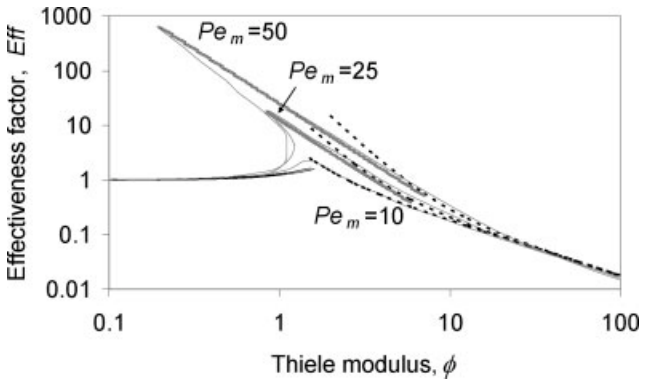

Figure 7. Effectiveness factor of a catalyst slab for a first-order chemical reaction.

Shown are the numerical results of Quinta Ferreira (1988, grey lines), the regular perturbation predictions for low Thiele modulus (solid black lines), the singular perturbation predictions for high Thiele modulus (dashed black lines) and the singular perturbation predictions for intermediate values of the Thiele modulus (thick grey lines), for $\gamma = 20$, $\beta = 0.1$ and $Pe_h = 5$.

agreement between the theoretical and numerical results in this regime for small β and $|\gamma\beta| < 2$. As $|\gamma\beta|$ is increased, the deviation between the theory and the numerics increases; the effectiveness factor is overestimated by the theory for $\beta > 0$ and underestimated for $\beta < 0$.

As a final note, we recall that in this work we have assumed the concentration and temperature at the surface of the catalyst slab to be known and fixed at $\hat{c}_s$ and $\hat{T}_s$, respectively. This presumes the external resistances to mass and heat transfer to/from the slab to be negligible. However, the findings in this paper also have relevance for situations in which these external resistances are significant. In such cases, only the concentration and temperature in the fluid at some distance from the slab will be known, respectively $\hat{c}_\infty$ and $\hat{T}_\infty$; but, the surface concentration and temperature are related to these through

$$-D\left.\frac{d\hat{c}}{d\hat{x}}\right|_{\hat{x}=L} = k_m(\hat{c}_s - \hat{c}_\infty) \tag{81}$$

$$-\kappa\rho C_p\left.\frac{d\hat{T}}{d\hat{x}}\right|_{\hat{x}=L} = h(\hat{T}_s - \hat{T}_\infty), \tag{82}$$

where k_m and h are the external mass transfer and heat transfer coefficients, respectively. Therefore, to calculate the concentration and temperature profiles inside the catalyst slab in the presence of external surface resistances, one needs an iterative procedure. One should start by guessing values for $\hat{c}_s$ and $\hat{T}_s$ (a good initial estimate is setting $\hat{c}_s = \hat{c}_\infty$ and $\hat{T}_s = T_\infty$), then use the results in Table 1 to calculate the internal concentration and temperature profiles and, finally, iterate estimating new values of $\hat{c}_s$ and $\hat{T}_s$ from Eqs. 81 and 82, respectively. The iteration should be repeated until the desired accuracy in $\hat{c}_s$ and $\hat{T}_s$ is achieved. We note that the external heat and mass transfer coefficients are unaffected by intraparticle convection, as demonstrated by the work of Stephanopoulos and Tsiveriotis,[7] mentioned earlier in the introduction section.

Conclusions

The interaction between transport of heat by conduction and convection, transport of reactants and products by diffusion and convection, and chemical reaction within a porous catalyst particle of slab geometry has been analyzed. A combination of perturbation and integral mathematical techniques was used to derive approximate analytical solutions for the concentration and temperature profiles, as well as for the maximum temperature and the effectiveness factor, for a first order, nonisothermal reaction. Three regimes of operation were characterized: regime I, in which convection and diffusion are dominant (small Thiele modulus, $\phi^2/Pe_m \ll 1$, $1/Pe_h$, $1/Pe_m$); regime II, in which diffusion and reaction are dominant (large Thiele modulus, $\phi^2/Pe_m \gg 1$, $1/Pe_h$, $1/Pe_m$); and regime III, in which convection and reaction dominate (intermediate Thiele modulus, $\phi^2/Pe_m \sim 1$, and $1/Pe_h$, $1/Pe_m \ll 1$). Our analytical solutions were validated by comparison with previous numerical results. It was shown that the maximum temperature inside the catalyst slab, as well as the maximum effectiveness factor, is achieved in regime III. Interestingly, the maximum temperature is equal to the temperature that would occur after complete, adiabatic reaction in a catalyst slab with initially uniform reactant concentration equal to the surface concentration of the slab operating in convective regime. To leading order, the maximum effectiveness factor is approximately proportional to the mass Peclet number and is independent of the heat Peclet number.

Notation

a = parameter defined in Eq. 86
A_1–A_5 = constants to be determined
b = parameter defined in Eq. 87
c = dimensionless concentration of reactant A
c_n = perturbation function of order n for dimensionless concentration
$\hat{c}$ = concentration of reactant A
$\hat{c}_s$ = concentration of reactant A at the surface of the slab
$\hat{c}_\infty$ = concentration of reactant A at some distance from the slab
C_p = specific heat of catalyst matrix filled with fluid
d = parameter defined in Eq. 88
D = effective coefficient of diffusion of reactant A within the porous matrix of the catalyst
E = activation energy for the reaction
Ei = Exponential integral function, defined by $Ei(z) = -\int_{-z}^{\infty}(e^{-t}/t)dt$ (for $z > 0$), where the principal value of the integral is taken
Eff = effectiveness factor
k = intrinsic kinetic constant of the reaction
k_m = external mass transfer coefficient
k_s = kinetic rate constant evaluated at the surface temperature of the catalyst
k_0 = preexponential factor in the Arrhenius rate law
h = external heat transfer coefficient
L = semi-thickness of the slab
p_0 = pressure at the entrance to the slab
Δp = pressure change across the catalyst slab
$Pe_h = uL/\kappa$ is the heat Peclet number
$Pe_m = uL/D$ is the mass Peclet number
q = heat of reaction
R = universal gas constant
T = dimensionless temperature
T_n = perturbation function of order n for dimensionless temperature
$\hat{T}$ = temperature
$\hat{T}_s$ = temperature at the surface of the slab
$\hat{T}_\infty$ = temperature at some distance from the slab
$(\Delta\hat{T})_{ad}$ = adiabatic temperature change

u = superficial velocity of the fluid inside the slab, which is assumed to be uniform
x = dimensionless transverse position within the slab
$\hat{x}$ = transverse position within the slab
X = stretched coordinate in the region near $x = 1$
Y = stretched coordinate in the region near $x = -1$
w = function defined in Eq. 42

Greek letters

$\beta = q\hat{c}_s D/(\rho C_p \hat{T}_s \kappa)$ is the Prater number
$\beta = \Delta p/p_0$ is the relative pressure change across the catalyst slab
ε = small parameter in perturbation expansion
$\phi = (k_s L^2/D)^{1/2}$ is the Thiele modulus
φ = parameter defined in Eq. 6a
$\gamma = E/(R\hat{T}_s)$ is the Arrhenius number
η = parameter defined in Eq. 6b
κ = effective thermal diffusivity of catalyst matrix filled with fluid
ρ = density of catalyst matrix filled with fluid

Subscripts

max = maximum
$n = 0, 1, 2, \ldots$ is the order of the perturbation function
s = surface of the slab

Superscripts

lb = left-hand-side boundary layer in the slab
lm = left and middle region in the slab
m = middle region in the slab
rb = right-hand-side boundary layer in the slab

Acknowledgments

This work was conducted during the Sabbatical leave of SSSC at the University of Porto. Travel funding from the EPSRC through grant EP/C547780/1 is gratefully acknowledged.

Literature Cited

1. Aris R. *The Mathematical Theory of Diffusion and Reaction in Permeable Catalysts*, *Vol.*1, *The Theory of Steady State*. Oxford: Clarendon, 1975.
2. Wheeler A. Reaction rates and selectivity in catalyst pores. *Adv. Catal.* 1951;3:249–327.
3. Komiyama H, Inoue H. Effects of intraparticle convective flow on catalytic reactions. *J Chem Eng Jpn.* 1974;7:281–286.
4. Nir A, Pismen L. Simultaneous intraparticle forced convection, diffusion and reaction in a porous catalyst. *Chem Eng Sci.* 1977;32:35–41.
5. Cogan R, Pipko G, Nir A. Simultaneous intraparticle forced convection, diffusion and reaction in a porous catalyst. *Chem Eng Sci.* 1982;37:147–151.
6. Cresswell D. Intraparticle convection: its measurement and effect on catalyst activity and selectivity. *Appl Catal.* 1985;15:103–116.
7. Stephanopoulos G, Tsiveriotis K. The effect on intraparticle convection on nutrient transport in porous biological pellets. *Chem Eng Sci.* 1989;44:2031–2039.
8. Lu ZP, Dias MM, Lopes JCB, Carta G, Rodrigues AE. Diffusion, reaction and convection in catalyst particles: analogy between slab and sphere geometries. *Ind Eng Chem Res.* 1993;32:1839–1852.
9. Afeyan N, Fulton S, Gordon N, Mazsaroff I, Varady L, Regnier F. Perfusion chromatography: an approach to purifying biomolecules. *Bio/Technology.* 1990;8:203–206.
10. Gordon N, Whitney D, Londo T, Nadler T. Affinity perfusion chromatography. *Methods Mol Biol.* 2000;147:1407–1413.
11. Regnier F. Perfusion chromatography. *Nature* 1991;350:634–635.
12. Tallarek U, Paces M, Rapp E. Perfusive flow and intraparticle distribution of a neutral analyte in capillary electrochromatography. *Electrophoresis* 2003;24:4241–4253.
13. Ghanem A, Shuler ML. Characterization of a perfusion reactor utilizing mammalian cells on microcarrier beads. *Biotechnol Prog.* 2000;16:471–479.
14. Kobayashi M, Togawa J, Kanno T, Horiuchi J, Tada K. Dramatic innovation of propene epoxidation of efficiency derived from a forced flow membrane reactor. *J Chem Technol Biotechnol.* 2003;78:303–307.
15. Veldsink J, Versteeg G, van Swaaij WP. An experimental study of diffusion and convection of multicomponent gases through catalytic and non-catalytic membranes. *J Membr Sci.* 1994;92:275–291.
16. Rodrigues AE, Quinta Ferreira R. Convection, diffusion and reaction in a large-pore catalyst particle. *AIChE Symp Ser.* 1988;84:80–87.
17. Lopes JCB, Dias MM, Mata VG, Rodrigues AE. Flow field and non-isothermal effects on diffusion, convection and reaction in permeable catalysts. *Ind Eng Chem Res.* 1995;34:148–157.
18. Bender CM, Orszag SA. *Advanced Mathematical Methods for Scientists and Engineers*. New York: Springer-Verlag, 1999.
19. Cardoso SSS, Rodrigues AE. Diffusion and reaction in a porous catalyst slab: perturbation solutions. *AIChE J.* 2006;52:3924–3932.
20. Quinta Ferreira RM. Contribuição Para o Estudo de Reactores Catalíticos de leito fixo. Efeito da Convecção em Catalisadores de Poros Largos e Casos de Catalisadores Bidispersos. PhD Thesis. Porto: University of Porto, 1988.
21. Satterfield CN. *Heterogeneous Catalysis in Practice*. New York: McGraw-Hill, 1980.
22. Rodrigues AE, Calo JM, Sweed NH, editors. *Multiphase Chemical Reactors—Design Methods*, *Vol.* 2. Rockville, MD: Sijthoff & Noordhoff, 1981. NATO ASI Series E-52.

Appendix

In this appendix, we derive the solutions for the concentration and temperature profiles in the catalyst particle in the boundary layer near $x = 1$, for regime II. Using the stretching transformation

$$X = (1 - x)\varepsilon^{-1/2} \tag{A1}$$

in the mass and energy balances (Eqs. 7–9) yields

$$-\varepsilon^{1/2}\frac{dc^{rb}}{dX} = \frac{1}{Pe_m}\frac{d^2c^{rb}}{dX^2} - \exp\left(\varphi\frac{T^{rb}}{1+\eta T^{rb}}\right)(c^{rb}+1) \tag{A2}$$

$$-\varepsilon^{1/2}\frac{dT^{rb}}{dX} = \frac{1}{Pe_h}\frac{d^2T^{rb}}{dX^2} + \exp\left(\varphi\frac{T^{rb}}{1+\eta T^{rb}}\right)(c^{rb}+1) \tag{A3}$$

with boundary conditions

$$c^{rb} = 0 \text{ and } T^{rb} = 0 \text{ at } X = 0 \tag{A4a, b}$$

where $c^{rb}(X)$ and $T^{rb}(X)$ refer to the concentration and temperature in the right-hand-side boundary layer. After expansion of $c^{rb}(X)$ and $T^{rb}(X)$ in a power series in $\varepsilon^{1/2} = \sqrt{Pe_m}/\phi$ and collection of terms of $O(1)$ in Eqs. A2 and A3, we obtain

$$\frac{1}{Pe_m}c_0^{rb} = -\frac{1}{Pe_h}T_0^{rb} + A_5 X \tag{A5}$$

$$0 = \frac{1}{Pe_h}\frac{d^2T_0^{rb}}{dX^2} + (1 + c_0^{rb})\ \exp\left(\varphi\frac{T_0^{rb}}{1+\eta T_0^{rb}}\right) \tag{A6}$$

where A_5 is a constant.

Matching the middle and right boundary layer solutions, we have

$$\lim_{X\to\infty} c_0^{rb} = \lim_{x\to 1} c_0^{m} = -1, \quad \varepsilon \to 0 \tag{A7}$$

and

$$\lim_{X\to\infty} T_0^{rb} = \lim_{x\to 1} T_0^{m}, \quad \varepsilon \to 0 \tag{A8}$$

Combining Eqs. A5 and A7, we expect

$$\lim_{X\to\infty} T_0^{rb} = \frac{Pe_{\mathrm{h}}}{Pe_{\mathrm{m}}}, \quad \varepsilon \to 0 \tag{A9}$$

and $A_5 = 0$.

Equation A6 is nonlinear and cannot be solved analytically in an exact manner. However, we may find an approximate solution. We expect

$$c_0^{rb} = -1 + w(X)$$
$$T_0^{rb} = \frac{Pe_{\mathrm{h}}}{Pe_{\mathrm{m}}}[1 - w(X)] \tag{A10a, b}$$

where $\lim_{X\to\infty} w(X) = 0$. From the boundary conditions, Eq. 36, we also have $\lim_{X\to 0} w(X) = 1$. Substituting Eq. A10b into Eq. A6 yields

$$0 = \frac{1}{Pe_{\mathrm{m}}}\frac{d^2w}{dX^2} - w\ \exp\left(\varphi \frac{Pe_{\mathrm{h}}}{Pe_{\mathrm{m}}}\frac{1-w}{1+\eta\frac{Pe_{\mathrm{h}}}{Pe_{\mathrm{m}}}(1-w)}\right) \tag{A11}$$

For small $\varphi Pe_{\mathrm{h}}/Pe_{\mathrm{m}}$ and $\eta Pe_{\mathrm{h}}/Pe_{\mathrm{m}}$, we may make the simplification

$$\exp\left(\varphi \frac{Pe_{\mathrm{h}}}{Pe_{\mathrm{m}}}\frac{1-w}{1+\eta\frac{Pe_{\mathrm{h}}}{Pe_{\mathrm{m}}}(1-w)}\right) \approx b^2 \tag{A12}$$

and treat b as approximately constant. Then $w(X) \approx e^{-b\sqrt{Pe_{\mathrm{m}}}X}$. Substituting this result into Eq. A10 gives

$$c_0^{rb} = -1 + e^{-b\sqrt{Pe_{\mathrm{m}}}X}$$
$$T_0^{rb} = \frac{Pe_{\mathrm{h}}}{Pe_{\mathrm{m}}}\left[1 - e^{-b\sqrt{Pe_{\mathrm{m}}}X}\right] \tag{A13a, b}$$

To determine b, we force the energy balance (Eq. A6) to be satisfied integrally in the whole of the boundary layer,

$$0 = \int_0^\infty \left[\frac{d^2T_0^{rb}}{dX^2} + \left(\frac{D}{\kappa} - T_0^{rb}\right)\ \exp\left(\varphi\frac{T_0^{rb}}{1+\eta T_0^{rb}}\right)\right]dX \tag{A14}$$

For small $\eta Pe_{\mathrm{h}}/Pe_{\mathrm{m}}$, Eq. A14 has solution

$$b = \left(\frac{e^{\varphi Pe_{\mathrm{h}}/Pe_{\mathrm{m}}} - 1}{\varphi Pe_{\mathrm{h}}/Pe_{\mathrm{m}}}\right)^{1/2} \tag{A15}$$

Manuscript received Sept. 20, 2006, and revision received Feb. 16, 2007.